

Electric Field Based Simulations of Local Oxidation Nanolithography using Atomic Force Microscopy in a Level Set Environment

Lado Filipovic ^{a,b} and Siegfried Selberherr ^a

^a Institute for Microelectronics, TU Wien,
Gußhausstraße 27–29/E360, A-1040 Wien, Austria

^b Christian Doppler Laboratory for Reliability Issues in Microelectronics
at the Institute for Microelectronics, Austria
Email: {filipovic|selberherr}@iue.tuwien.ac.at

During the last decades it has been shown that non-contact AFM can be used as an efficient lithographic technique capable of manufacturing nanometer sized devices on the surface of a silicon wafer. The AFM nanooxidation approach is based on generating a potential difference between a cantilever needle tip and a silicon wafer. A water meniscus builds up between the tip and the wafer, resulting in a medium for oxyions to move due to the high electric field in the region. A simulator for nanooxidation with non-contact AFM tools, implemented in a Level Set environment, was developed. The presented model uses empirical equations for the height and half-width of an AFM nanodot or nanowire with a physics based shape model. The shape model uses a particle distribution directly derived from the surface charge density, generated on the silicon surface due to the strong electric field.

Introduction

Conventional photolithographic methods, which are derived from optical and electron beam lithographies, are no longer capable of providing the necessary processing steps for the fabrication of modern nanosized devices. They are either too cost intensive or unsuitable for handling the extensive variety of organic and biological systems applicable to nanotechnology (1). Furthermore, conventional process simulation models are unable to describe the steps required to generate structures manufactured on the nanoscale. During the last decades, alternatives to conventional photolithography were actively investigated, such as nanoimprint lithography (2), soft lithography (3), and scanning probe lithography (4). The most promising method for nanofabrication was found to be scanning probe oxidation, or Local Oxidation Nanolithography (LON). The reasons behind the success of LON are bountiful, among the most important being its ability to be performed at room temperature and across a large range of materials.

Local Oxidation Nanolithography

The development of LON originated with the development of the scanning probe microscope in the 1980s. Scanning Tunnel Microscopy (STM) was developed in 1982 (5), followed by Atomic Force Microscopy (AFM) in 1986 (6), as methods to utilize tunneling current and/or electrostatic forces between a conductive cantilever tip and a sample surface in order to detect and measure depressions and protuberances on a nanometer sized section of a sample surface. AFM has been used extensively, not only in

the semiconductor industry, but also in physics, chemistry, biology, biochemistry, and other disciplines where the chemical or physical properties of a surface are required (7). Several years later, local anodic oxidation of semiconductor surfaces was suggested by Dagata et al. (4) as a method to modify semiconductor surfaces with nanoscale precision. In their pioneering work, Dagata et al. used a STM microscope in order to generate features with 100nm resolution by applying a potential difference between the STM needle tip and a silicon surface. More recently LON has been studied and improved for use as a patterning tool for the deposition, removal, and modification of material surfaces with nanoscale precision (8), (9), (10). After the initial work with a STM microscope, similar processes have been reported using an AFM microscope with a conductive probe attached to a cantilever in contact and non-contact modes (9), (10). A distinct advantage of AFM over STM is its ability to read back the actual topography of the generated pattern, while STM is unable to show the real height. In addition, the advantage of non-contact mode AFM over contact mode AFM is the increased reliability of the AFM needle tip (11). Contact mode AFM causes the needle tip to degrade much faster due to the repeated contact with the semiconductor surface during operation. The models presented here deal with LON patterns generated with an AFM device operating in non-contact mode, as this was found to be the most promising method for generating narrow patterns at relatively high speeds.

Level Set Method

The presented LON simulator functions fully alongside the process simulator presented in (12). The Level Set (LS) method is utilized in order to describe the top surface of a semiconductor wafer as well as surfaces which separate different materials. The LS method describes a movable surface S as the zero LS of a continuous function, defined on the entire simulation domain,

$$S(t) = \{\vec{x} : \Phi(\vec{x}, t) = 0\}. \quad [1]$$

The implicitly defined surface S describes a surface evolution, driven by a scalar velocity $v(x)$, using the LS equation

$$\frac{\partial \Phi}{\partial t} + V(\vec{x}) \|\nabla \Phi\| = 0, \quad [2]$$

where $\Phi=0$ denotes the location of the surface S on the entire simulation domain. In order to find the velocities $v(x)$ when simulating LON patterning, a Monte Carlo technique is implemented: a desired number of particles are distributed and accelerated towards the silicon wafer surface. The collision of particles with the surface identifies the location where the surface must be advanced by a desired rate. The distribution of particles determines the shape of the generated nanopattern. For more details regarding the implementation of the LS method and the parallelization technique for the LS simulator, please refer to (12), (13). The next sections describe the implementation of the AFM nanodot and nanowire models, followed by a derivation of the quantile function for electric-field dependent particle distribution, and simulation results are presented.

Modeling of Non-Contact AFM Nanodots and Nanowires

As shown in Figure 1 (a), the first step of nanopatterning with AFM is the application of a voltage bias to the tip of an AFM needle and bringing the needle in close proximity to a substrate surface. Due to the high electric field generated in the region and the relative humidity of the ambient, a water meniscus (or water bridge) is formed, providing an electrolyte between the needle (cathode) and the sample surface (anode). The presence

of the water meniscus limits the lateral diffusion of anions, thereby limiting the lateral extensions of the AFM nanodot. Inside the water meniscus, oxyanions (OH^-) are generated due to the high electric field. The oxyanions then undergo an oxidation reaction through interaction with the silicon surface. For a silicon wafer, the oxidation reaction, including holes (h^+) and electrons (e^-), at the anode end (silicon surface) is



while the reaction at the cathode end (AFM needle tip), from (1) is



There is a variety of factors which affect the geometry of a generated nanodot or nanowire, such as pulse time, applied bias voltage, relative humidity, and tip shape. Three types of AFM tip shapes have been analyzed in the literature (14). The different shapes are for a rough, hemispherical, and blunt tip configuration, which can be modeled using a ring charge, point charge, and line charge, respectively. The presented model assumes a hemispherical tip shape, which means that it can be modeled by replacing the AFM needle with an effective point charge Q and observing the electric field generated with this charge, as shown in Figure 1 (b). For the implemented model, it is assumed that all oxyanions are generated at the effective point source of the AFM needle tip. This simplifies the model, while not having a significant consequence on the model's accuracy (15). The oxyanions traverse through the water meniscus along electric field lines, finally colliding with the sample surface, where oxidation is initiated.

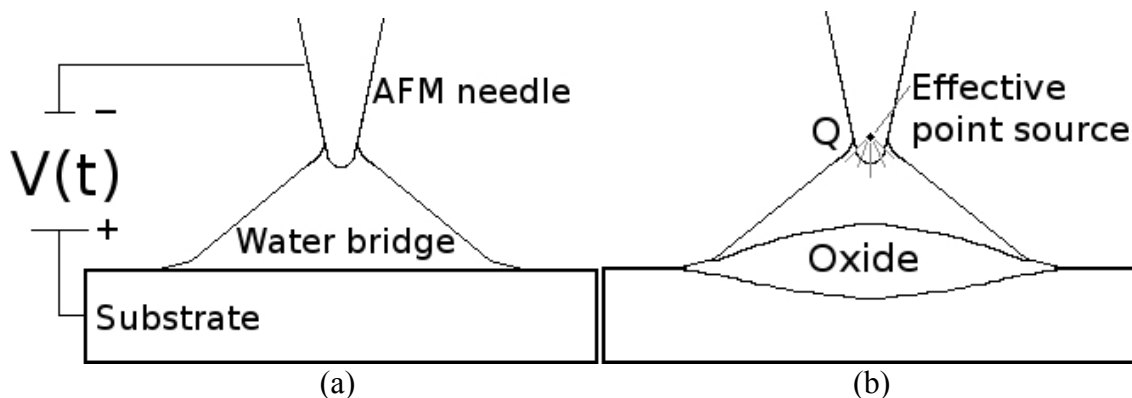


Figure 1. (a) Basic schematic for LON with an AFM needle and (b) the simulation model, which treats the AFM needle as a point charge.

Neglecting the effects of surrounding ions on the electric field strength and recombination reactions between ions to form water, the voltage and electric field strength in the water meniscus region can be calculated using the image charge method (14), (15), (16). Mesa et al. (16) suggest that each AFM needle can be represented as a series of charged particles distributed along the structure of the needle. The presented model implements the simplest form of this model with the use of a single point charge, valid for hemispherical AFM needles. The electric field is then calculated and the Surface Charge Density (SCD) distribution along the substrate surface is found. The oxyanion distribution along the silicon surface drives the oxidation reaction; therefore, the shape of an AFM generated nanodot follows the SCD distribution.

Image Charge Method for Generating the Surface Charge Density Distribution

As discussed in the previous section, the model representing the shape of an AFM generated nanodot follows the SCD distribution, which is derived by replacing the AFM

needle tip with an effective point source Q and the silicon substrate surface by an infinitely long conducting plane. The image charge method is then applied to find the voltage at every location in the water meniscus region $p(x,y,z)$:

$$V(\vec{p})=k\left[\frac{Q}{(x^2+y^2+(z-D)^2)^{1/2}}-\frac{Q}{(x^2+y^2+(z+D)^2)^{1/2}}\right], \quad [5]$$

where $k=1/4\pi\epsilon_r\epsilon_0$, Q is the effective point charge at a distance D from the surface, and ϵ_r is the relative permittivity of water. Given $\vec{E}=-\vec{\nabla}V$ the electric field strength can be found:

$$\begin{aligned} E_x &= \frac{-\partial V}{\partial x} = kQ \left[\frac{x}{(x^2+y^2+(z-D)^2)^{3/2}} - \frac{x}{(x^2+y^2+(z+D)^2)^{3/2}} \right], \\ E_y &= \frac{-\partial V}{\partial y} = kQ \left[\frac{y}{(x^2+y^2+(z-D)^2)^{3/2}} - \frac{y}{(x^2+y^2+(z+D)^2)^{3/2}} \right], \\ E_z &= \frac{-\partial V}{\partial z} = kQ \left[\frac{z-D}{(x^2+y^2+(z-D)^2)^{3/2}} - \frac{z+D}{(x^2+y^2+(z+D)^2)^{3/2}} \right]. \end{aligned} \quad [6]$$

The induced SCD on the surface is represented as $\sigma(x,y,0)=\epsilon_r\epsilon_0 E_z(x,y,0)$, leading to the expression

$$\sigma(x,y,0)=\frac{-DQ}{2\pi(x^2+y^2+D^2)^{3/2}}. \quad [7]$$

A model has already been developed which utilizes expression [7] in order to generate a topographical representation of an AFM nanodot (17). However, the model implements a Monte Carlo rejection technique to build the nanodot, which is very time and processing resource expensive, when large aspect ratio problems are required. Large aspect ratios are a common concern for nanopatterning simulations, since a very small part of a relatively large wafer surface requires modifications.

Empirical Models for AFM Nanodots and Nanowires

AFM Nanodot. In (18) empirical equations describing the influence of the bias voltage (V) and pulse time (t) on the height (H) and half-width (W) of an AFM generated nanodot have been presented:

$$\begin{aligned} H(V,t) &= (-2.1+0.5V-0.006V^2)+(0.1+0.03V-0.0005V^2)\ln(t), \\ W(V,t) &= (11.6+9V)+(2.7+0.9V)\ln(t). \end{aligned} \quad [8]$$

Expression [8] fails to address the effects of relative humidity on the AFM nanodot height and half-width. The true effects of relative humidity on LON have been debated in various publications (14), (19), (20), (21). The general consensus is that the relative humidity influences the size of the generated water meniscus, which in-turn has an effect on the nanodot size. This effect has been added to the presented AFM nanodot model.

AFM Nanowire. In (21) the dimensional characteristics of an AFM generated nanowire was studied as a function of the applied voltage, oxidation time, humidity, and crystalline orientation. The conclusions that were drawn were collected and an empirical model for the height and half-width of an AFM nanowire was developed (22). The simulator presented in (22) uses a particle distribution based on the well known Gaussian and Lorentzian profiles in order to generate AFM nanodots and nanowires. It is the aim of this work to use the SCD distribution on the substrate surface in order to generate a particle distribution, which is presented in the following section.

SCD Based Particle Distribution Modeling

One-Dimensional SCD Distribution

When performing AFM nanodot simulations for a two-dimensional model, a one-dimensional particle distribution is required. Equation [7] can be re-written in a one-dimensional form:

$$\sigma(x, 0) = \frac{-DQ}{2\pi(x^2 + D^2)^{3/2}}. \quad [9]$$

[9] is used in order to generate a one-dimensional Probability Density Function (PDF)

$$f(x) = -C \frac{DQ}{2\pi(x^2 + D^2)^{3/2}}. \quad [10]$$

where C is the normalization constant. C is found by integrating $f(x)$ over the entire simulation domain and equating it to one:

$$\int_{-\infty}^{\infty} f(x) dx = -C \int_{-\infty}^{\infty} \frac{DQ}{2\pi(x^2 + D^2)^{3/2}} dx = 1. \quad [11]$$

Solving [11], we find that $C = -\pi D/Q$, which is then substituted into [10] to form the normalized PDF for a one-dimensional SCD distribution

$$f(x) = \frac{D^2}{2(x^2 + D^2)^{3/2}}. \quad [12]$$

The next step is finding the Cumulative Probability Distribution (CPD) function, derived by integrating the normalized PDF, $\Phi(r) = \int_{-\infty}^r f(x) dx$, where r is the SCD distributed radius. Because of the symmetry of the SCD distribution on either side of the charged particle Q , generating a CPD distributed radius becomes easier, when $-0.5 \leq \Phi(r) \leq 0.5$.

Therefore, we set $\Phi(r) = \int_0^r f(x) dx$, leading to

$$\Phi(r) = \xi = \int_0^r f(x) dx = \int_0^r \frac{D^2}{2(x^2 + D^2)^{3/2}} dx = \left(\frac{r}{2\sqrt{r^2 + D^2}} \right). \quad [13]$$

Setting $\Phi(r)$ equal to an evenly distributed random number $\xi \in [-0.5, 0.5]$ and inverting the CPD function from [13] allows to obtain the SCD quantile function required for particle generation:

$$r = 2D \frac{\xi}{\sqrt{1 - 4\xi^2}}. \quad [14]$$

Therefore, in order to generate particles obeying the SCD distribution along the silicon wafer surface, each particle must be generated using [14], where ξ is an evenly distributed random number, $\xi \in [-0.5, 0.5]$.

Two-Dimensional SCD Distribution

When working with a three-dimensional model for AFM nanodots, a two-dimensional particle distribution is required. The analysis is similar to the one-dimensional model presented in the previous section. The derivation of the quantile function is performed using polar coordinates for simplicity and for easier generation of a final radial distribution of particles. For polar coordinates (r_n, θ) it is important to note that $x^2 + y^2 = r_n^2$ and $dx dy = r_n dr_n d\theta$. The two-dimensional PDF is

$$f(x, y) = -C \frac{DQ}{2\pi(x^2 + y^2 + D^2)^{3/2}} \rightarrow f(r_n, \theta) = -C \frac{DQ}{2\pi(r_n^2 + D^2)^{3/2}}, \quad [15]$$

The normalization constant C is found by the same procedure used for the one-dimensional model, to be $C=-I/Q$ and the normalized two-dimensional PDF becomes

$$f(r_n, \theta) = \frac{D}{2\pi(r_n^2 + D^2)^{3/2}} \quad [16]$$

The cumulative probability distribution is then found by integrating the normalized PDF, $\Phi(r) = \int_0^{2\pi} \int_0^r f(r_n, \theta) r_n dr_n d\theta$, where r is the SCD distributed radius. The quantile function for the two-dimensional SCD distribution is then found by inverting the SCD function to obtain

$$r = D \sqrt{\frac{1}{(1-\xi)^2} - 1}, \quad [17]$$

where ξ is an evenly distributed random number, $\xi \in [0,1]$.

Non-Contact AFM Nanodot and Nanowire Simulations

AFM Nanodot

The AFM nanodots shown in Figure 2 were generated using the described model from (18) with added humidity effects and the two-dimensional SCD distribution explained in the previous sections. The nanodots show, how the topography of a silicon surface is modified after AFM application with various bias voltages. The ambient humidity is set to 55% and the pulse time to 0.125ms. The top surface represents the interface between the AFM oxide nanodot and the ambient, while the bottom surface represents the interface between the AFM oxide nanodot and the silicon substrate.

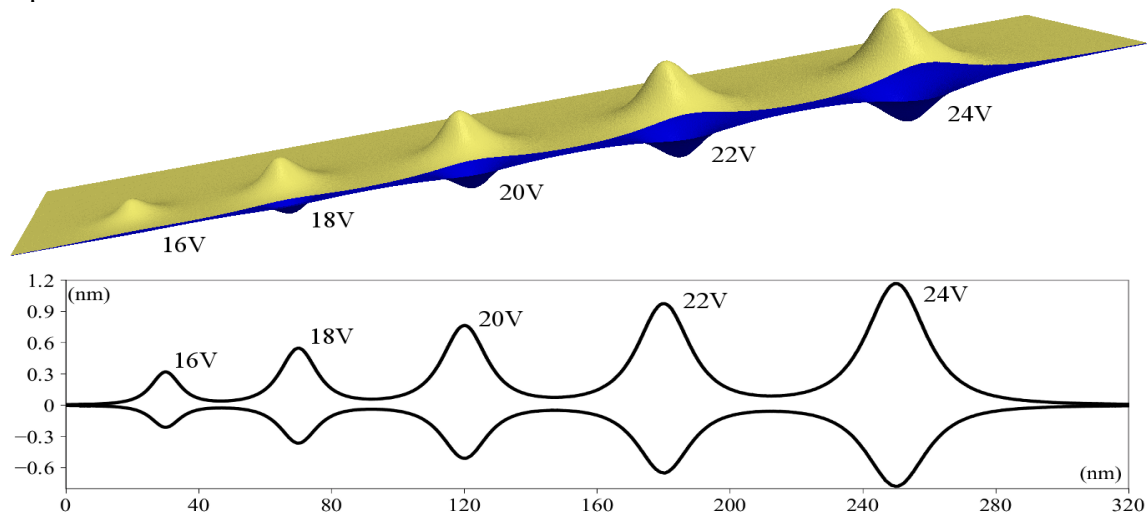


Figure 2. The effect of voltage variation for AFM generated nanodot heights and widths.

AFM Nanowire as a Sequence of AFM Nanodots

In (18) it is suggested that a nanowire, which is patterned using a combination of AFM nanodots, separated at 0.5nm intervals will have an increased half-width due to the increased time for the lateral diffusion of anions. This phenomenon was added to the simulator and a nanodot was generated in the LS simulator to mimic the one presented in (18), as is shown in Figure 3. As in (18), generating nanodots with 20V pulses for 1ms, while displacing the tip laterally by 0.5nm resulted in a nanowire with a height of approximately 1nm and a half-width of 13nm. This type of simulation, which generates a nanowire as a combination of many nanodots, requires long simulation times. An alternative is to model a nanowire as a single topography-changing process, which is the method implemented for the generation of the nanowires shown in Figure 4.

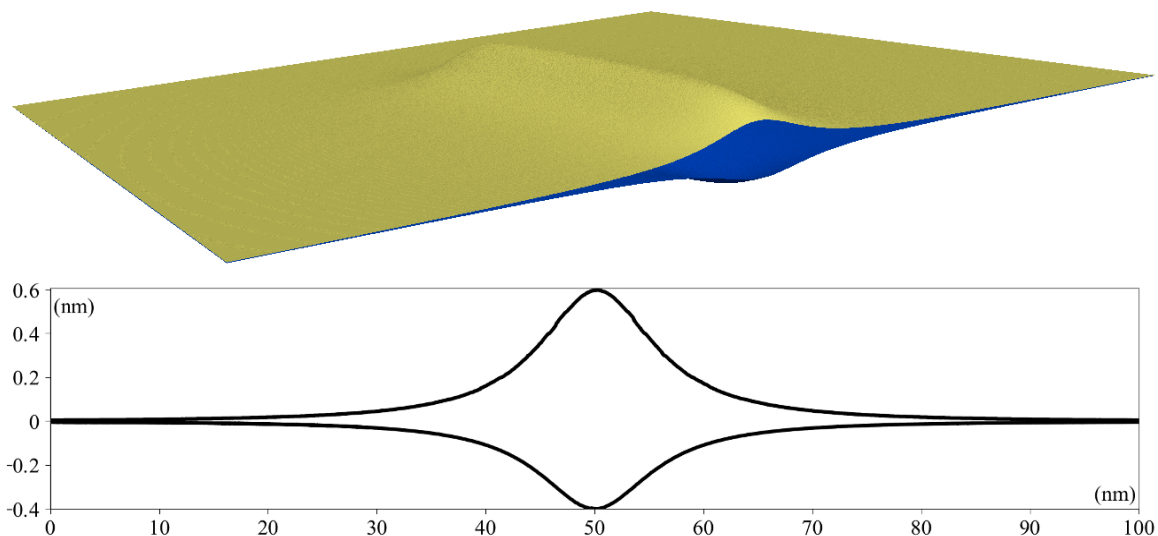


Figure 3. Nanowire topography simulated using a sequence of AFM nanodots (top) and the nanowire's cross-section (bottom).

AFM Nanowires

Instead of generating nanowires as a series of nanodots, an approach using empirical equations which govern nanodot height and half-width under various conditions, from (21) was implemented in the simulator. This type of simulation is much quicker as it allows for a nanowire to be treated as a single simulation step as opposed to thousands of single nanodot generation steps. The nanowires also exhibit a shape based on the SCD distribution. Figure 4 shows nanowires generated using the sample from (21) at bias voltages ranging from 6V to 10V, with a 5ms pulse time and 72% humidity.

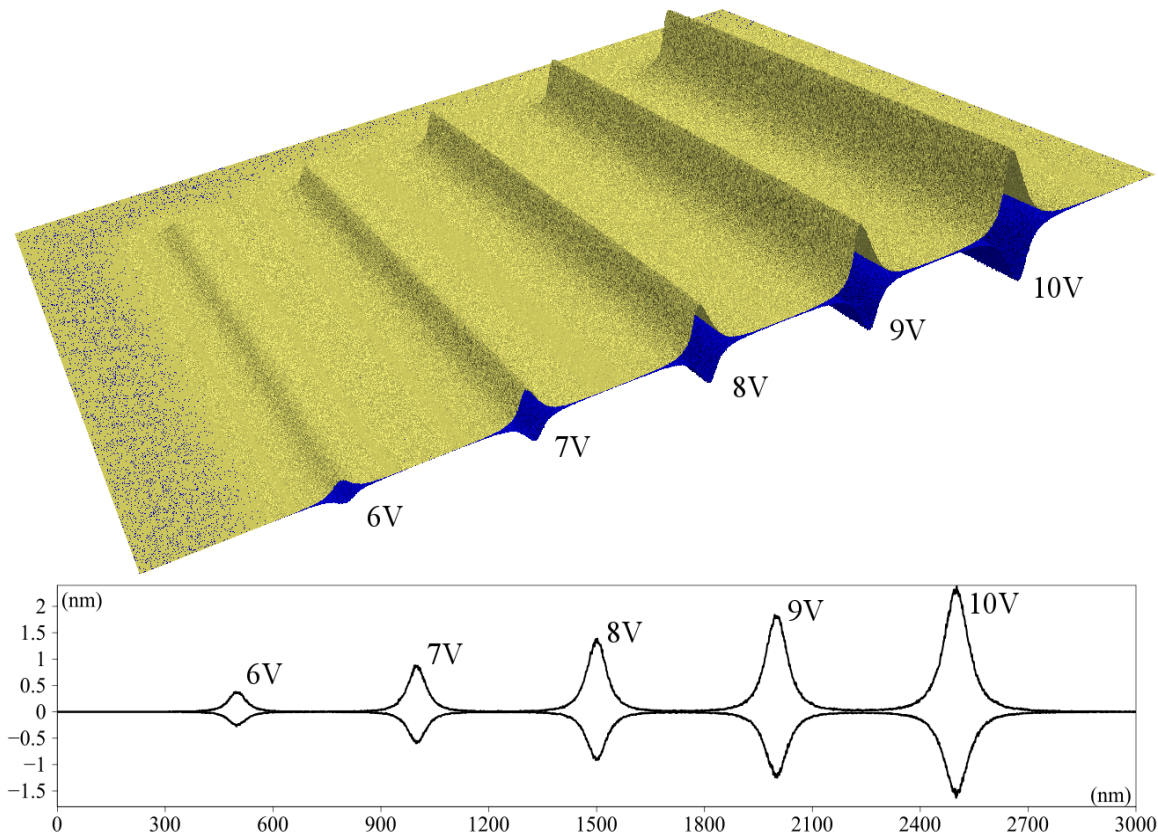


Figure 4. Nanowires generated using the model from (21) with a SCD distribution.

Conclusion

Local oxidation nanolithography implemented with an AFM microscope has proven to be a useful tool for the generation of nanosized patterns on a silicon wafer surface. A model for the generation of nanodots and nanowires with non-contact AFM tools is presented and integrated into a LS based process simulator. The AFM needle tip provides a voltage bias, which leads to the generation of a water meniscus between the needle and the sample surface. An electric field is generated within the water meniscus, causing the generation of oxyanions (OH^-) and accelerating them towards the silicon, where an oxidation reaction is initiated. The tip is assumed to be hemispherical, which allows it to be modeled as a single charged particle suspended a certain distance away from the silicon surface. A quantile function for the resulting surface charge density distribution is derived and is implemented within the model in order to generate the shape of desired nanodots and nanowires. This function is derived for a one-dimensional and a two-dimensional SCD distribution, which makes the model useful for two-dimensional and three-dimensional AFM simulations, respectively. The integration of the topographical simulation of nanopatterns generated with AFM into the LS simulator enables easy integration of further simulation steps, such as photolithography, CVD, and chemical wet etching in order to generate a desired device within the same simulation environment.

References

1. R. Garcia, R.V. Martinez, and J. Martinez, *Chem. Soc. Rev.*, **35**, p. 29 (2006).
2. S.Y. Chou, P.R. Krauss, and P.J. Renstrom, *Science*, **272**, 5258, p. 85 (1996).
3. Y. Xia and G.M. Whitesides, *Angew. Chem. Int. Ed. Engl.*, **37**, 5, p. 551 (1998).
4. J.A. Dagata et al., *Appl. Phys. Lett.*, **56**, p. 2001 (1990).
5. G. Binnig, H. Rohrer, and C. Gerber, *Phys. Rev. Lett.*, **49**, p. 57 (1982).
6. G. Binnig, C.F. Quate and G. Gerber, *Phys. Rev. Lett.*, **56**, p. 930 (1986).
7. Q. Tang, S.Q. Shi and L. Zhou, *J. Nanosci. Nanotechnol.*, **4**, 8, p. 948 (2004).
8. R.V. Martinez et al., *Nano Lett.*, **7**, p. 1846 (2007).
9. G. Qin and C. Cai, *Nanotechnology*, **20**, 35, p. 355306 (2009).
10. A. Notargiacomo and A.A. Tseng, *Nanotechnology*, (IEEE-NANO), p. 907 (2009).
11. D. Stievenard, P.A. Fontaine, and E. Dubois, *Appl. Phys. Lett.*, **70**, p. 3272 (1997).
12. O. Ertl and S. Selberherr, *Comp. Phys. Comm.*, **180**, 8, p. 1242 (2009).
13. L. Filipovic, O. Ertl, and S. Selberherr, in *Parallel and Distributed Computing and Networks*, M. Resch and A. Toptsis, Editors, PDCN Proceedings, Innsbruck, Austria (2011).
14. S. Djurkovic et al., *Surf. Sci.*, **601**, 23, p. 5340 (2007).
15. A. Orians et al., *Surf. Sci.*, **600**, 16, p. 3297 (2006).
16. G. Mesa, E. Dobado-Fuentes and J.J. Saenz, *J. Appl. Phys.*, **79**, p. 39 (1996).
17. L. Filipovic and S. Selberherr, *LNCS 2011*, **7116**, p. 447 (2011).
18. M. Calleja and R. Garcia, *Appl. Phys. Lett.*, **76**, 23, p. 3427 (2000).
19. P. Avouris, T. Hertel, and R. Martel, *Appl. Phys. Lett.*, **71**, 2, p. 285 (1997).
20. H. Kuramochi, K. Ando, and H. Yokoyama, *Surf. Sci.*, **542**, 1, p. 56 (2003).
21. T.H. Fang, *Microelectronics Journal*, **35**, 9, p. 701 (2004).
22. L. Filipovic and S. Selberherr, *Intl. Conf. on Simulation of Semiconductor Processes and Devices*, (SISPAD), p. 307, Osaka, Japan (2011).